Beamforming vs. Near-Field Acoustic Holography

Thiago Henrique Gomes Lobato[1], Roland Sottek[2], Michael Vorländer[3]
[1] HEAD acoustics GmbH, 52134 Herzogenrath, Email: thiago.lobato@head-acoustics.de
[2] HEAD acoustics GmbH, 52134 Herzogenrath, Email: roland.sottek@head-acoustics.de
[3] IHTA Institut für Hörtechnik und Akustik, 52074 Aachen, Email: mvo@akustik.rwth-aachen.de

Introduction

Both beamforming and **n**ear-field **a**coustic **h**olography (NAH) are microphone array-based techniques that are used to estimate source locations and their strengths in various application areas [1-3]. Although some of their acoustical fundamentals are the same, the ways the two methods and their variations approach the problem of source identification and quantification are unique. Hence, in practical applications it is necessary to have a very clear understanding of what to expect from each method. This paper describes the main variations of the two approaches: the delay-and-sum beamforming, also known as conventional beamforming (CB), and the **F**ourier-based planar **n**ear-field **a**coustic **h**olography (FNAH), highlighting the differences and similarities between the two approaches and recommending their use for different situations. To illustrate their difference, known results from analytical equations of a baffled piston and a vibrating plate are used.

Beamforming

Beamforming in its general form is a technique that uses signals from sensor arrays to perform spatial filtering. The idea is to define a looking direction and to remove most of the signal coming from any other direction.

The delay-and-sum beamforming algorithm works by delaying each signal and then averaging all of the microphones in the array. Thus, sounds from a particular direction add coherently while others are incoherently summed, thereby amplifying all signals from that particular direction. The required delay for each microphone in the array can be estimated by acoustic source models, often monopoles [2,4], the model used in this work.

This operation can be performed in the frequency domain and can be derived from the following relationship for a single source from direction i [4]:

$$\boldsymbol{p_i} = a_i \cdot \boldsymbol{g_i} \tag{1}$$

where a_i is the source strength, $\boldsymbol{p_i}$ the complex pressure in the frequency domain and $\boldsymbol{g_i}$ is called the steering-function that contains information about the source i.

To identify the source auto strength $\mathrm{A}_i = |a_i|^2$ for each direction i in a multi-source situation (I sources), a least-squares solution for each direction can be obtained as [4]:

$$|a_i|^2 \approx \widetilde{\mathrm{A}}_i = 0.5 \cdot \frac{\boldsymbol{g_i^* p p^H g_i}}{|\boldsymbol{g}_i|^4} = \boldsymbol{w_i^* C w_i} \tag{2}$$

$$\boldsymbol{w_i} = \frac{\boldsymbol{g_i}}{|\boldsymbol{g_i}|^2} \tag{3}$$

where $\boldsymbol{C}$ is the signal cross-spectral matrix and $\widetilde{\mathrm{A}}_i$ the least-squares solution. The relation between $\widetilde{\mathrm{A}}_i$ and A_i is as follows [2]:

$$\widetilde{\mathrm{A}}_i = A_i + \sum_{j=1, j\neq i}^{I} A_j |\boldsymbol{g_j^H w_i}|^2 \ . \tag{4}$$

The sum term in Equation (4) is the interference term coming from sources in unwanted directions. This relationship is very important to note, as it shows that the beamforming result neither exactly represents the sources nor a real surface pressure, but rather the value that is achieved after spatial filtering of the signal with the goal of identifying a source in a certain direction. For well-isolated sources, enough microphones, and a relatively fine grid, the source strength can be calculated in the correct position with practically no errors. The term $\left|\boldsymbol{g_j^H w_i}\right|^2$ becomes smaller the more microphones used and the higher the incoherence of the steering functions.

Near-field acoustic holography

Near-field **a**coustic **h**olography (NAH) is a technique that directly reconstructs either an acoustic pressure field or a velocity field, whereby, for example, strongly vibrating regions can be identified. It is very effective in characterizing radiating acoustic surfaces.

The **F**ourier-based planar **n**ear-field **a**coustic **h**olography (FNAH) describes the pressure/velocity field in a given plane with Fourier spatial basis functions (angular spectrum) [1]. For a vibrating surface with velocity $\dot{w}$, the pressure p for different reconstruction surfaces can be derived from the following relationship [5]

$$p = \mathcal{F}^{-1} G_N \mathcal{F}\, \dot{w} \tag{5}$$

where $\mathcal{F}$ is a two-dimensional Fourier transform operator that maps the velocity/pressure onto the K-space representation (angular spectra) and G_N is a propagation operator that accounts for the different plane locations of the source and the reconstructed pressure. For the case of a radiating surface in the X-Y plane with plane waves, the above operators are defined as:

$$\mathcal{F} = \int\int e^{-jk_x x} e^{-jk_y y}\, dx\, dy \tag{6}$$

$$\mathcal{F}^{-1} = \left(\frac{1}{2\pi}\right)^2 \int\int e^{jk_x x} e^{jk_y y}\, dx\, dy \tag{7}$$

$$G_N = \frac{\rho c k}{k_z}\ e^{jk_z d} \tag{8}$$

where k is the wave number, ρ the density of air, c the speed of sound, d the positive distance in the z-direction between the source and reconstruction plane and $k_z = \sqrt{k^2 - k_x^2 - k_y^2}$. For reasons of efficiency, the 2D discrete

Fast-Fourier-Transform algorithm with window is often used to calculate $\mathcal{F}$. In this work, we used a 2D Hamming window. If $k^2 < k_x^2 + k_y^2$, the G_N term drops exponentially with distance, which makes it very difficult to inversely propagate the measured pressure. The type of waves that generate this effect are called evanescent waves and are one of the main challenges facing FNAH [5]. To take this problem into account, all FNAH calculations in this paper are regularized with a Tikhonov regularization with regularization parameter $\lambda_T = 0.5$, unless explicitly stated.

Technical acoustics example

This section describes the most important formulations for the acoustic problems used in this work.

Baffled circular piston

The baffled circular piston is a classic problem in acoustics [6]. It is defined as finding the pressure at a given point created by a vibrating piston at a steady velocity on a rigid baffle, as seen in Figure 1

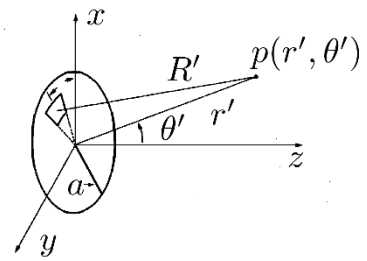

Figure 1: Schematic representation of the baffled circular piston problem [6].

The solution of this problem is the Rayleigh integral:

$$\mathrm{p}(r', \theta') = \frac{\mathrm{i}\rho\omega}{2\pi} \mathrm{U}_0 \int \frac{\mathrm{e}^{-\mathrm{ikR}'}}{R'} \mathrm{dS}\,, \tag{9}$$

where U_0 is the piston velocity, ω the angular frequency and S the piston surface.

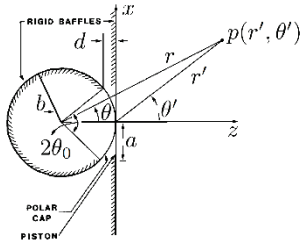

Figure 2: Schematic representation of the polar-cap radiation problem. The solution to this problem converges to the circular rigid piston problem by $\lim \boldsymbol{b} \to \infty \equiv \lim \boldsymbol{d} \to \mathbf{0}$.

Equation (9) does not have a single closed form solution for any r' and θ'. An exception is for $\theta' = 0$, for which the problem has the following closed form solution [6]:

$$p(r', \theta' = 0) = -\rho c U_0 \cdot \left(e^{-ik\sqrt{r'^2 + a^2}} - e^{-ikr'} \right) \tag{10}$$

Exact solutions for the integral can be achieved by region-dependent series expansions [7] or by calculating limiting cases that converge to the exact solution [8]. In this work, the second approach is used by taking into account the limiting polar cap radiation problem as indicated in [8] and presented in Figure 2.

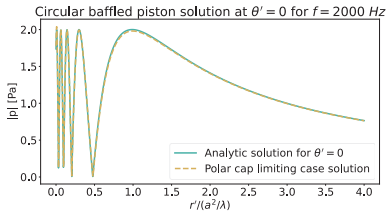

Figure 3: Comparison between the closed form solution of the baffled acoustic piston at $\boldsymbol{\theta' = 0}$ and the limiting solution of the polar cap for $\boldsymbol{a = 0.8}$ m. It is possible to see that the polar cap converges to the correct piston solution.

The analytical solution of the polar cap problem is the series expansion defined as (P_n: Legendre polynomial of order n, h_n: spherical Hankel function of order n, $2\theta_0$: opening angle of polar cap):

$$p(r, \theta) = \frac{\rho c U_0}{2i} \sum_{n=0}^{\infty} \frac{\left[P_{n-1}(cos(\theta_0)) - P_{n+1}(cos(\theta_0))\right]}{h_n'(kb)} \cdot h_n(kr) P_n(cos(\theta)) \tag{11}$$

An example of this limiting solution can be seen in Figure 3 for $a = 0.8$, $f = 2000$ Hz, $\theta_0 = \theta' = 0$ and $\lambda = 2\pi/k$.

Finite simply supported vibrating plate

One possible model for the perpendicular motion function $w(\boldsymbol{x})$ of a thin simply supported plate, which is driven by a point force in its surface, can be given by the following differential equation [1]:

$$\nabla^4 w(\boldsymbol{x}, \omega) - k_f^4 w(\boldsymbol{x}, \omega) = \frac{1}{D} F(\omega) \delta(\boldsymbol{x} - \boldsymbol{x_0}) \tag{12}$$

where D is the flexural rigidity of the plate $D = Eh^3/\left(12 \cdot (1 - \nu^2)\right)$, E is the Young's Modulus, ν the Poisson Modulus, h is the plate thickness, $\boldsymbol{x}$ is the position vector in (x, y), $F(\omega)$ the frequency dependent force, $\delta(\cdot)$ the Dirac delta function, k_f the bending wavenumber defined as $k_f = (\rho_s h \omega^2 / D)^4$ and ρ_s the plate density.

With the help of the modal expansion for the plate, it is possible to solve for the velocity as a function of the plate modes:

$$\dot{w}(\boldsymbol{x}, \omega) = j\omega \frac{F}{\rho_s h} \sum_{m=1}^{\infty} \sum_{n=1}^{\infty} \frac{\Phi_{mn}(\boldsymbol{x_0}) \Phi_{mn}(\boldsymbol{x})}{\omega^2 - w_{mn}^2} \tag{13}$$

w_{mn} being the natural frequency of the plate for the m and n mode defined as:

$$w_{mn} = \alpha^2 \cdot \left[(m\pi/L_x)^2 + \left(n\pi/L_y\right)^2 \right] \tag{14}$$

The Skudrzyk's plate constant is defined as $\alpha = \left(\frac{D}{\rho_s h}\right)^{1/4}$. L_x and L_y are the dimensions of the rectangular plate and the mode shapes are equal to:

$$\Phi_{mn}(\boldsymbol{x}) = \frac{2}{\sqrt{L_x L_y}} sin(m\pi x/L_x) sin\left(n\pi y/L_y\right) \tag{15}$$

In this work, the radiation from the plate is evaluated numerically from the velocity field according to Equation (5). For all later calculations a rectangular (square) microphone array with 1 m length and a distance of 0.025 m between the microphones was used.

Type of array

The two methods use microphone arrays, but as mentioned earlier, they solve the identification of acoustic radiation problems in different ways. For Fourier based near-field acoustic holography, ideally the array should have equally spaced microphones, so the 2D FFT algorithm can be used for efficient performance. For this reason, most of the arrays used for the planar FNAH are evenly spaced microphones placed on a grid. In addition, the array should encompass (at least) the entire source so the leakage effect of the 2D FFT is minimal. In practice, different measurements are often combined with a single small array.

For the delay-and-sum beamforming, one of the main goals of the array design is to minimize the interference term in Equation (4). To achieve this, array geometries such as spirals [3] or optimized scatter points [4] are used. Often, an equally spaced grating array will not give the best side-lobe reduction, so there are better solutions for beamforming with the same number of microphones, although the same array can be used for the two methods.

Results of the two methods

Although the two methods can be used to identify prominent radiation regions, each method achieves this with a different approach. By using CB, the power of a theoretical source radiating from the looking direction plus the contribution of sources radiating from other directions that could not be completely removed is preserved. FNAH does not seek the strength of a source, but rather an equivalent velocity or pressure surface that generates the measured signals.

This difference can be very well illustrated using the example of plate radiation. The example involves exciting a thin steel plate of $h = 3\,mm$ at 300 Hz, $\boldsymbol{x_0} = (-0.05, -0.15)$ and measuring at 0.1 m distance. The normalized resulting velocity field can be seen in Figure 4 along with the result of using FNAH and CB.

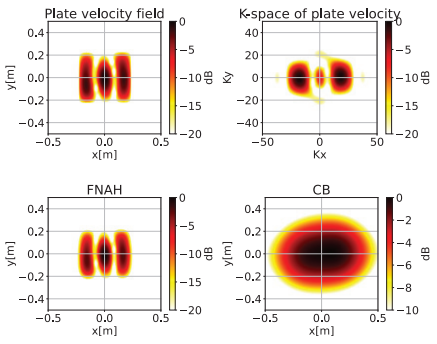

Figure 4: Normalized velocity field of a point driven thin plate. Vibrating plate with point source excitation at 300 Hz for FNAH and CB at **z = 0.1 m**. The result of FNAH closely matches the actual velocity field of the plate.

Here it can be seen that the FFT near-field-acoustic holography reconstructs the velocity surface on the one hand, while on the other hand, the beamforming merges all radiation surfaces into one large source, since the radiating surfaces are too close to each other to be spatially separated.

This conceptual difference can lead to very interesting results in some examples, such as for the baffled piston. For a case with $a = 0.4\,m$ and $f = 2000$ Hz, the results of different planes for the two methods can be seen in Figure 5.

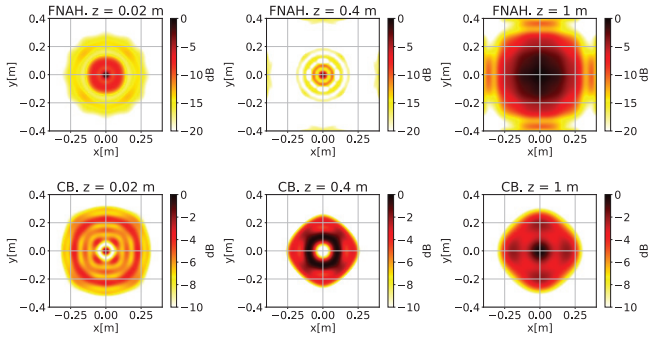

Figure 5: Baffled piston results at different distances for both FNAH and CB method.

From the results we can see that although the holography always has a maximum velocity in the center of the piston, the beamforming maximum changes drastically depending on the distance. The positions where the interference is strong in the center of the piston correlate to the places of destructive pattern on the near-field main axis of radiation, as shown in an example in figure 3. The reason for this is that the CB model does not take into account the strong near-field interferences, so that only sources in an outer circle are found at positions where the interference pattern destroys the sources in the center of the piston. This is especially good for far-field evaluations, but not so good for identifying surface values. At 1 m, the two methods are closer to the far field, and the FNAH result can only be achieved with a stronger regularization ($\lambda_T = 5$), so that hardly any evanescent wave is propagated back.

Frequency influence

For the FNAH, better resolution is achieved at lower frequencies, while for beamforming the higher frequencies provide better resolution. This is due to the fact that for radiations with low frequencies, the Fourier spatial basis often also has a lower spatial wave number and therefore the pressure does not have to be scanned in a fine grid. This can easily be seen in the plate example by looking at the velocity pattern at 1 kHz in Figure 6, which has much more high frequency components than at 300 Hz, which can be seen by comparing their K-space representation.

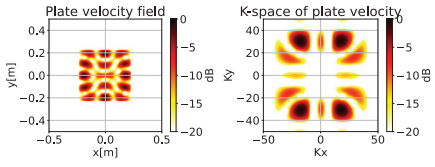

Figure 6: Plate velocity field at 1 kHz. This pattern shows much more high frequency spatial components than at 300 Hz (see Figure 4).

For delay-and-sum beamforming, on the other hand, the resolution is higher when the interference term is minimal.

This is the case at high frequencies when the transfer functions of different directions add more destructively due to their very different phase values. This can be easily illustrated by comparing the phase of some points for a microphone array with a rectangular grid for a similar rectangular scanning grid in Figure 7.

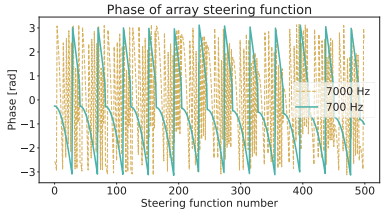

Figure 7: Phase of steering functions for a low (700 Hz) and a high (7000 Hz) frequency for some points from a uniform rectangular microphone array and scanning grid (1 m away).

Near field vs. far field

As the name suggests, NAH is ideally used for near-field measurements to reveal the nuances of the acoustic field. Due to the evanescent waves, however, measurements in the far field will be extremely sensitive to noise and regularization will be required. To show this, the example calculated above for the baffled piston at z = 1 m without and with regularization ($\lambda_T = 5e3$) for a noise case with a (complex) Gaussian white noise with a signal-to-noise-ratio (SNR) of 20 dB is calculated and the results can be seen in Figure 8.

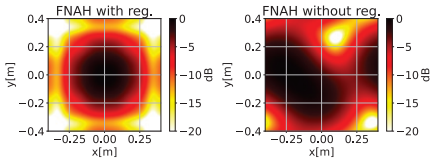

Figure 8: FNAH result for baffled piston at z=1 m with and without regularization for a SNR of 20 dB.

The calculation without any regularization is destroyed because the noise increases exponentially.

Beamforming is much more robust against noise and works exceptionally well in the far field. Using beamforming to calculate the same example as above but with a significantly lower SNR of 5 dB, still gives a very reasonable result, as can be seen in Figure 9.

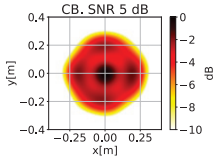

Figure 9: CB result for the baffled piston at z=1 m for a SNR of 5 dB.

Conclusion

In this paper we have described both the delay-and-sum beamforming and the Fourier based near-field acoustic holography and presented their main differences for two technical acoustics example sources: a baffled vibrating piston and a thin plate. From the plate example it could be seen that the FNAH result is close to the correct surface velocity, but the CB filters the signal spatially, so that only a general location of the radiating source could be estimated. In the case of the piston, beamforming was able to identify the complex interference patterns as a function of distance, indicating from which direction the sound can be detected at each position. The FNAH remained somewhat similar for the different locations with its maximum velocity at the center of the piston.

The type of array appropriate for each method is also different. The main goal of the beamforming array design is to minimize the interference of unwanted directions, while the FNAH array is often composed of equally spaced microphones, so the 2D FFT algorithm can be applied efficiently. Additionally, the FNAH array should ideally encompass the entire sound source (although many measurements can be combined for stationary sources if using a reference microphone).

The influence of the frequency and sound field was also assessed. For the FNAH, lower frequency radiation patterns can be estimated more easily due to their lower spatial frequencies, while for CB higher frequencies are more advantageous due to the smaller interference term, since the transfer functions between different distances are less correlated. The FNAH only works well in the near field due to the evanescent waves, while beamforming can also be used in the far field, although it is unable to reconstruct real surface velocities, which could be of great importance in some applications.

With respect to noise the CB is more robust against lower SNR ratios than FNAH.

Literature

[1] Williams, E.G.: Fourier Acoustics: Sound Radiation and Nearfield Acoustical Holography, Academic Press, 1999
[2] Sijtsma, P. et al.: High-resolution CLEAN-SC: Theory and experimental validation; International Journal of Aeroacoustics, 16(4-5), 274-298, March 2017
[3] Arcondoulis, E.J.G. et al.: A Modification to Logarithmic Spiral Beamforming Arrays for Aeroacoustic Applications. Proceedings of the 17th AIAA/CEAS Aeroacoustics Conference (32nd AIAA Aeroacoustics Conference), Portland, Oregon, June 2011
[4] Merino-Martínez, R., Snellen, M. and Simons, D.G.: Functional Beamforming Applied to Imaging of Flyover Noise on Landing Aircraft. Journal of Aircraft: devoted to aeronautical science and technology, 53(6), 1830-1843, June 2016
[5] Williams, E.: Regularization methods for near-field acoustical holography, J. Acoust. Soc. Am. 110(4), 1976-1983, October 2001
[6] New, R., Becker, R.I. and Wilhelmij, P.: A limiting form for the nearfield of the baffled piston, J. Acoust. Soc. Am., 70(5), 1518-1526, November 1981
[7] Mast, T.D. and Yu, F.: Simplified expansions for radiation from a baffled circular piston, J. Acoust. Soc. Am. 118(6), 3457-3464, December 2005
[8] Malgoezar, A. et al.: Improving beamforming by optimization of acoustic array microphone positions, Proceedings of the 6th Berlin Beamforming Conference, BeBeC, February 2016.